Growth kinetics and electronic properties of unintentionally doped semi-insulating GaN on SiC and high-resistivity GaN on sapphire grown by ammonia molecular-beam epitaxy

Tang, H.; Fang, Z.Q.; Rolfe, S.; Bardwell, J.A.; Raymond, S.

Publisher's version / Version de l'éditeur:
https://doi.org/10.1063/1.3415527
JOURNAL OF APPLIED PHYSICS, 107, 103701, pp. 1-11, 2010-05-18

Growth kinetics and electronic properties of unintentionally doped semi-insulating GaN on SiC and high-resistivity GaN on sapphire grown by ammonia molecular-beam epitaxy

H. Tang,[1,a] Z. Q. Fang,[2] S. Rolfe,[1] J. A. Bardwell,[1] and S. Raymond[1]
[1]*Institute for Microstructural Sciences, National Research Council Canada, Ottawa, Ontario K1A 0R6, Canada*
[2]*Semiconductor Research Center, Wright State University, Dayton, Ohio 45435, USA*

(Received 27 November 2009; accepted 26 March 2010; published online 18 May 2010)

Growth of unintentionally doped (UID) semi-insulating GaN on SiC and highly resistive GaN on sapphire using the ammonia molecular-beam epitaxy technique is reported. The semi-insulating UID GaN on SiC shows room temperature (RT) resistivity of 10^{11} Ω cm and well defined activation energy of 1.0 eV. The balance of compensation of unintentional donors and acceptors is such that the Fermi level is lowered to midgap, and controlled by a 1.0 eV deep level defect, which is thought to be related to the nitrogen antisite N_{Ga}, similar to the "EL2" center (arsenic antisite) in unintentionally doped semi-insulating GaAs. The highly resistive GaN on sapphire shows RT resistivity in range of 10^6–10^9 Ω cm and activation energy varying from 0.25 to 0.9 eV. In this case, the compensation of shallow donors is incomplete, and the Fermi level is controlled by levels shallower than the 1.0 eV deep centers. The growth mechanisms for the resistive UID GaN materials were investigated by experimental studies of the surface kinetics during growth. The required growth regime involves a moderate growth temperature range of 740–780 °C, and a high ammonia flux (beam equivalent pressure of 1×10^{-4} Torr), which ensures supersaturated coverage of surface adsorption sites with NH_x radicals. Such highly nitrogen rich growth conditions lead to two-dimensional layer by layer growth and reduced oxygen incorporation. © *2010 American Institute of Physics*. [doi:10.1063/1.3415527]

I. INTRODUCTION

Semi-insulating or high-resistivity GaN materials are required for important device applications such as high power, high frequency transistors, and diodes. Because of strong tendency of acquiring n-type residual impurities and native defects such as oxygen and nitrogen vacancies, it has always been a challenge to achieve insulating GaN materials by various growth methods. Various approaches have been employed to compensate these residual donors by intentional doping with Mg, C, Fe, etc. Among them, carbon doping and iron doping methods are demonstrated as effective doping schemes to obtain semi-insulating GaN with all major growth techniques such as hydride vapor phase epitaxy (HVPE),[1,2] metal-organic chemical vapor deposition (MOCVD) (Refs. 3–5) and molecular-beam epitaxy (MBE).[6–8] Intentionally doped GaN played important role in the development of nitride based electronics. The heavily doped semi-insulating GaN materials are mainly used as thick buffer layers in GaN HEMT devices. However, concern still exists as to possible deterioration of electrical or optical performance associated with carrier trapping, short effective carrier lifetime,[9] growth quality degradation, or memory effect of the compensation impurities. In that regard, unintentionally doped (UID) semi-insulating or high-resistivity GaN have advantages especially when used for the active regions of devices such as HEMT, PIN diodes, and high voltage Schottky diodes, and when efficiency associated with long carrier lifetime is required.

There have been reports of UID high-resistivity GaN grown by various growth techniques. The high-resistivity UID GaN materials grown by MOCVD generally contain high carbon concentrations and high dislocation densities.[4] High-resistivity UID GaN was also reported for the plasma-assisted MBE technique but few details on growth mechanisms and no electrical data on "semi-insulating" status GaN have been reported.[10–12] There have been also several reports of high resistivity UID GaN on grown on SiC or sapphire substrates with the ammonia-MBE technique.[13,14] Again, no detailed study of electrical properties and mechanisms analysis has been reported. In fact, high-resistivity UID GaN has been routinely grown on silicon wafers by ammonia-MBE, as part of the GaN HEMT-on-silicon recipe developed by a group in France.[15–17] However, the limited resistivity (usually in the order of 10^4 Ω cm) of the resistive silicon substrate itself prevented accurate study of the resisitivity and compensation mechanisms of the GaN epilayers.

In the present article, we report achievement of UID semi-insulating GaN on SiC and high-resistivity GaN on sapphire using the ammonia-MBE growth technique. The ideal growth conditions were analyzed with help of investigation into the basic growth kinetics of the ammonia-MBE process. The electrical properties and defect levels were studied by temperature dependent dark current (TDDC) measurements and thermally stimulated current (TSC) spectros-

[a]Author to whom correspondence should be addressed. Electronic mail: haipeng.tang@nrc.ca.

copy. SIMS and photoluminescence data were also collected to facilitate the interpretation of the electrical properties.

II. EXPERIMENTAL METHODS

The growth system used for this study is an SVTA nitride MBE (model N35S) equipped with an ammonia injector with ammonia flow capacity up to 200 SCCM (SCCM denotes cubic centimeter per minute at STP). The system also features carbon-doping capability using a saddle-field low energy ion source and methane source gas.[18] The substrate temperatures were calibrated by pyrometer measurements. In order to understand a wide range of growth parameters and growth regimes reported for ammonia-MBE growth by various authors, we performed an experimental study of ammonia cracking and nitride surface incorporation kinetics using the hydrogen surface desorption spectroscopy methodology. The desorbed hydrogen from ammonia cracking on a stationary or a growing GaN surface (i.e., with or without Ga flux supplied) was measured by a quadruple mass spectrometer. The difference of the hydrogen partial pressure measured when the ammonia flux is directed on the surface and when the ammonia flux is shuttered away is treated as a measure of the amount of the hydrogen released from the ammonia surface cracking and lattice incorporation reactions. In order to cover a wide range of growth conditions reported in the literature, and especially to understand the conditions to grow high-resistivity GaN materials, measurements were performed for a wide range of temperatures from 300 to 900 °C, and ammonia flux from 5 to 200 SCCM. The Ga flux, when applied, was fixed at a beam equivalent pressure (BEP) of 1.1×10^{-6} Torr corresponding to a growth rate of about 1 μm/hr.

2 in. sapphire and 4H SiC substrates (both repolished by NOVASIC Inc.) were used for the growth experiments. For both types of substrate, the cleaning procedure before loading for growth includes flushing by boiled chloroform vapor, hydrogen fluoride (HF) dip and 10 min deionized (DI) water rinse and drying by nitrogen. Ideal growth conditions for achieving semi-insulating or high-resistivity GaN were found to include high ammonia flux, appropriate temperature window, and two-dimensional (2D) growth mode. In order to understand the different growth mechanisms for both highly resistive and conducting GaN layers, GaN samples have been grown under varied growth temperature and ammonia flux to represent the most typical growth regimes used in practical growth. For both sapphire and SiC substrates, a 1000 Å thick AlN grown at 900 °C was used as a buffer layer. *In situ* reflection high energy electron diffraction (RHEED) was used to monitor the growth mode during growth. Both conducting and insulating GaN layers grown have been analyzed by secondary ion mass spectroscopy (SIMS), atomic force microscopy (AFM), and low temperature PL (photoluminescence). PL spectra were measured at 10 K with a He–Cd laser excitation at wavelength of 325 nm. The electrical properties and defect mechanisms in the semi-insulating or high-resisitivity GaN samples were investigated using TDDC measurements, photoconductivity measurements, and TSC spectroscopy.

III. AMMONIA CRACKING KINETICS AND GROWTH REGIMES

For ammonia MBE growth, the active nitrogen species are provided by the thermal cracking of the ammonia molecules incident on the growing surface. In order to understand the growth mechanisms with the ammonia MBE technique, it is crucial to understand the cracking behavior of ammonia molecules. In a study of GaN selective area growth, Gupta *et al.* measured ammonia cracking efficiency on various substrate materials without incident Ga flux, using the hydrogen desorption method. Mesrine *et al.*[20] studied ammonia cracking efficiencies by monitoring the optical reflectivity of predeposited Ga thin (a few monolayers) layers during exposure to an ammonia flux. The latter study has determined ammonia cracking efficiency as a function of temperature from 250 up to 830 °C under an incident Ga flux. It has shown that the cracking efficiency becomes significant above 450 °C and reaches about 3.8% or slightly more for temperatures above 700 °C. Crawford *et al.*[21] have studied both gallium and hydrogen desorption using the desorption mass spectroscopy technique. They have found that under Ga rich growth conditions, the excess gallium adatoms block adsorption sites for ammonia, and thus reduce the growth rates. Based on these studies and other growth data, Karpov *et al.*[22] developed a detailed surface kinetics model for interpretation of available experimental and growth data. This model assumes an adsorption layer consisting of gallium adatoms and adsorbed NH_x radicals. The model takes into account specific effects of the blocking of NH_3 adsorption sites by the coverage of these surface species.

In the present work, we measured the ammonia cracking efficiency using the hydrogen desorption method for a wide range of temperature and ammonia flux parameters covering most typical growth regimes reported in the literature. Particularly, we obtained experimental data for the difference of ammonia cracking efficiencies on a GaN surface with or without an incident Ga beam for a wide temperature range. Such data help to provide insight into the different growth mechanisms for the different growth regimes reported in the literature.

Figure 1 shows the ammonia cracking efficiency on stationary GaN surface (without incident Ga flux), as represented by the desorbed hydrogen pressure, as a function of the incident ammonia flux at various substrate temperatures. This graph shows the saturation of cracking with increasing ammonia flux. This confirms the assumption by Karpov *et al.*[22]that saturated adsorption sites blocks further adsorption of ammonia molecules. A new ammonia molecule can be adsorbed only if an adsorption site is replenished after a pair of NH_x radicals recombine and are desorbed as N_2 and H_2. Since the desorption rate of the NH_x radicals is thermally activated, the ammonia cracking efficiency on nongrowing, stationary GaN surface shows strong temperature dependence.

In Fig. 2, for a fixed ammonia flux of 70 SCCM (BEP $=3.5\times10^{-5}$ Torr), the desorbed hydrogen pressure is measured as a function of temperature. In Fig. 2(a), one set of data is for cracking measurement on nongrowing GaN sur-

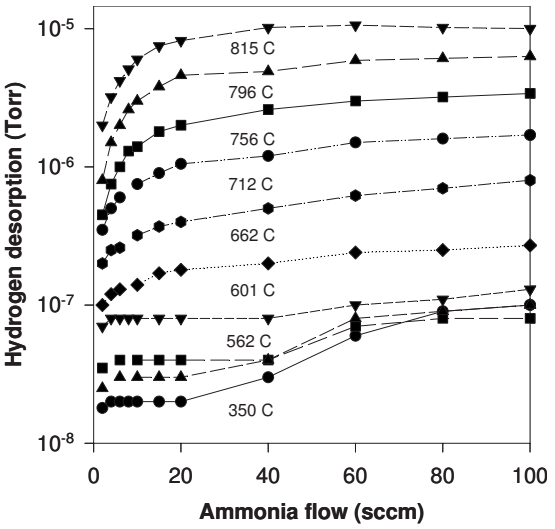

FIG. 1. Ammonia cracking efficiency on stationary GaN surface (without incident Ga flux), as represented by the desorbed hydrogen partial pressure, as a function of the incident ammonia flux at various substrate temperatures.

face, and the other set is for growing GaN surface with incident Ga flux corresponding to BEP of 1.1×10^{-6} Torr (equivalent to 1 μm/hr). Noticeably, in the lower temperature range (<800 °C), the reaction between Ga adatoms and NH_x radicals, which results in GaN lattice incorporation, greatly increased the hydrogen desorption rate. However, the two curves approach each other toward the high temperature end (>800 °C). To illustrate this trend more clearly, the difference is taken by subtracting the two curves and replotted in Fig. 2(b). The data shown in Fig. 2(b) can be understood as the contribution to hydrogen desorption due to Ga atoms reacting with an adsorbed NH_x radical. The reaction leads to hydrogen release and GaN lattice growth. The reaction also speeds up the replenishing rate of the adsorptions sites, since the sites blocked by adsorbed NH_x radicals become new available adsorption sites following the $Ga+NH_x \Rightarrow GaN+H_2$ reaction. That explains the increase in ammonia cracking with an incident Ga beam over most of the temperature range in Fig. 2(a).

Figure 2(b) reveals three temperature zones of different characteristics. We find that these zones can be related to the different growth regimes used by various authors in the practical growth work. The low temperature Zone I (350 to 550 °C) the differential hydrogen desorption rate shows a quick decline below 550 °C. This indicates that the reaction efficiency between Ga adatoms and adsorbed NH_x radicals becomes insufficient to cause 100% lattice incorporation of the Ga adatoms. As a result, metal gallium accumulates on the surface, blocking nitrogen adsorption sites, and reducing the growth rate. The reduction of growth rate under Ga rich conditions has been well documented and interpreted in Refs. 21–23.

In zone II (550 to 800 °C), the differential hydrogen desorption rate is basically constant with temperature, within the margin of error for the measurement method used. This means that in this temperature range, the $Ga+NH_x \Rightarrow GaN+H_2$ reaction rate is constant, limited by the fixed Ga incident flux. In the entire zone II, and especially in the lower

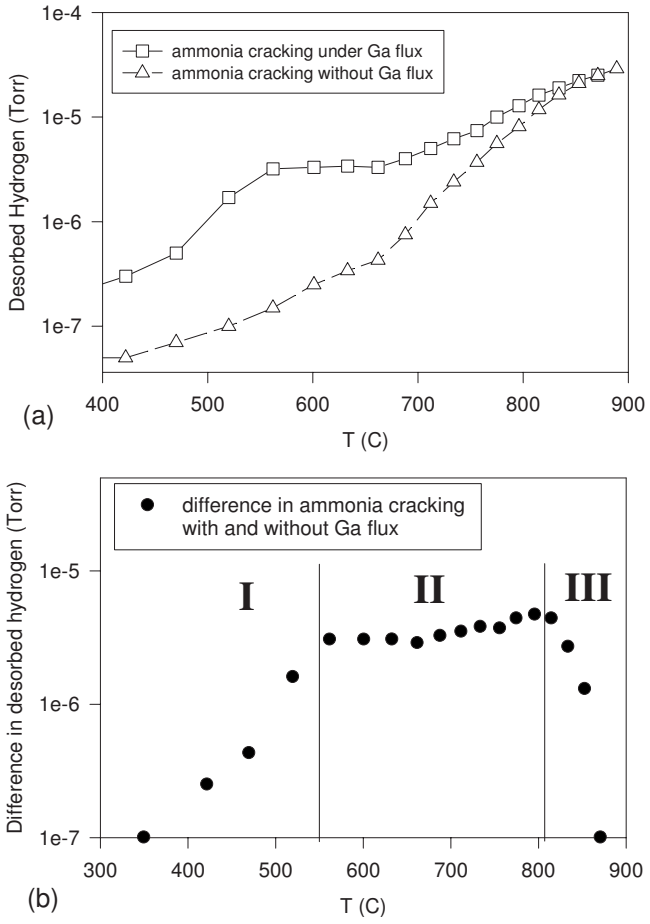

FIG. 2. (a) Cracking efficiency of ammonia (70 SCCM, BEP=3.5×10^{-5} Torr) on GaN surface as represented by desorbed hydrogen partial pressure as a function of temperature, measured with or without an incident Ga flux (BEP=1.1×10^{-6} Torr), and (b) Difference between the ammonia cracking efficiencies with and without the Ga flux.

temperature portion, Ga sticking coefficient is close to unity, i.e., minimal re-evaporation rate. The growing GaN surface is still saturated with adsorbed NH_x radicals over the entire temperature range of zone II. This is the typical nitrogen rich growth regime where growth rate is constant and depends only on Ga flux.

In zone III (800 to 900 °C), we observe a rapid drop of the differential hydrogen desorption rate when the temperature increases above 800 °C. This is because of the significantly elevated ammonia self-cracking rate associated with the $NH_x+NH_x \Rightarrow N_2+H_2$ reaction, which is now faster than and dominates over the $Ga+NH_x \Rightarrow GaN+H_2$ lattice incorporation reaction in this high temperature range. This can be seen from Fig. 2(a). The desorbed hydrogen pressure on stationary GaN surface without incident Ga increased to 2×10^{-5} Torr at 880 °C, which far exceeded the maximum hydrogen release pressure of about 3×10^{-6} Torr due to GaN incorporation as indicated by the plateau level in both Figs. 2(a) and 2(b). We can see the two curves in Fig. 2(a) approaches each other in this high temperature range. This means that GaN incorporation is no longer a rate-limiting event for ammonia cracking. Instead, the adsorbed NH_x radicals are desorbed rapidly via $NH_x+NH_x \Rightarrow N_2+H_2$ reaction, resulting in very short dwell time on the adsorption sites. In

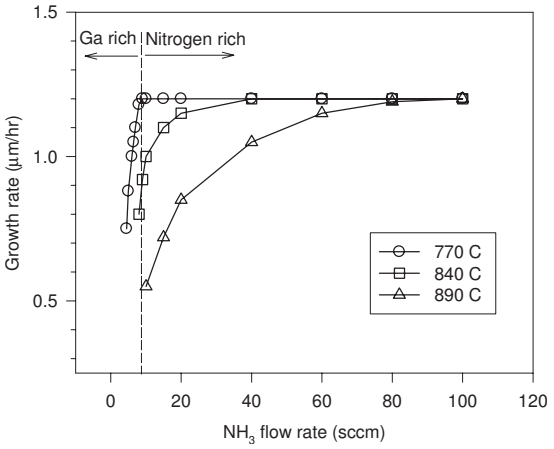

FIG. 3. For a given Gallium flux (BEP=1.3×10^{-6} Torr) and several substrate temperatures, the nitrogen rich to gallium rich transition point is determined from the change in the measured growth rate on varying the nitrogen flux.

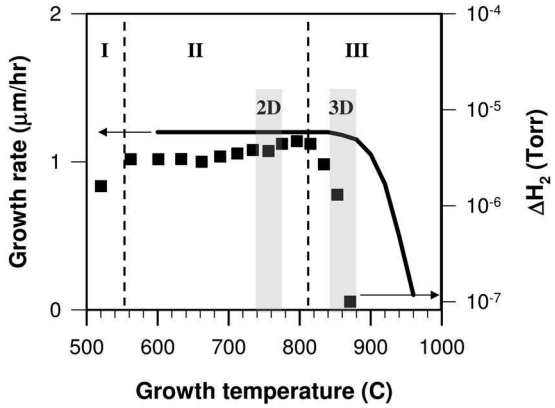

FIG. 4. The characteristics of nitrogen rich growth as a function of growth temperature for ammonia flow rate of 100 SCCM (BEP=5×10^{-5} Torr) and Gallium flux of BEP=1.3×10^{-6} Torr. The hydrogen desorption data in Fig. 2(b) are redrawn and overlapped with the growth rate characteristics here.

other words, the self desorption of the adsorbed nitrogen species (independent of the reaction with Ga) is fast enough so that the adsorption sites on the GaN surface are no longer saturated or blocked by them. This is a very important feature for growth performed in zone III, as opposed to growth performed in zone II. In this article, we will attempt to associate practical growth results, especially the growth mechanisms of semi-insulating GaN materials with the surface kinetics features discussed here.

Practical growth of GaN materials and devices by ammonia MBE has been performed by various groups using a range of temperature and ammonia flux parameters. These parameters generally fall into several growth regimes optimized for different purposes on the material. Zone I (350 to 550 °C) conditions in Fig. 2(b) have rarely been applied to any practical growth, except maybe for attempt to grow InN or InGaN materials. Most practical growth regimes are nitrogen rich growth, where the growth rate is constant, and limited only by the supplied Ga flux.

For a given gallium flux (BEP=1.3×10^{-6} Torr), on varying the nitrogen flux, the nitrogen rich to gallium rich transition point can be observed from the change in the measured growth rate. As shown in Fig. 3, at moderate temperature of 770 °C, the growth rate is constant when ammonia flow rate is greater than 8 SCCM but drops abruptly when the ammonia flow is decreased below 8 SCCM. The transition at 8 SCCM ammonia (BEP=4.5×10^{-6} Torr) corresponds to V/III=1 condition where V represents cracked and incorporated ammonia flux. The transition from nitrogen-rich to Ga-rich growth results in gallium surface accumulation and reduction in growth rate.[21–23] For higher substrate temperatures, as shown in Fig. 3, this transition becomes less abrupt because the gallium sticking probability can no longer be assumed to be unity.

The characteristics of nitrogen rich growth as a function of growth temperature are illustrated in Fig. 4. With ammonia flux set at 100 SCCM (BEP=5×10^{-5} Torr), the growth rate is constant up to about 880 °C, beyond which the growth rate starts to drop due to GaN thermal decomposition and accelerated desorption of adsorbed species.

In a previous paper, we analyzed some of the most frequently seen growth regimes in the literature.[24] Historically, in the authors' laboratory, a growth regime using a high temperature (840–880 °C) just below the GaN thermal decomposition threshold point and a moderate ammonia flux (100 SCCM, BEP=5×10^{-5} Torr) has been established and applied for GaN high-electron-mobility transistors (HEMT) devices on sapphire and SiC substrates.[25,26] In this growth regime, the growth is via a three-dimensional (3D) mode, yielding facetted surface morphology but also large grain size, low defect density, and high electron mobility, mainly due to the higher growth temperature used.[25] Unintentionally doped GaN grown in this regime is always n-type conducting. As a solution, we developed a carbon doping method using a low energy methane ion source, which successfully compensates all residual donors and yields semi-insulating GaN materials required for the HEMT devices.[18] On the other hand, another growth regime employing a moderate growth temperature (740–780 °C) and high ammonia flux (≥200 SCCM, BEP≥1×10^{-4} Torr) has been established for the development of GaN HEMT on Si (111) wafers.[15–17] Growth in this regime is via 2D mode, yielding excellent surface and interface smoothness. In addition, the GaN layers grown in this regime are highly resistive without any intentional doping, satisfying the requirement of resistive buffer layers for HEMT devices.[15–17] Similar layer-by-layer growth conditions have also been used for growth of GaN/InGaN or GaN/AlGaN quantum well structures (on sapphire substrates) where interface smoothness is important.[27–29]

In Fig. 4, we marked on the growth rate curve with shadow windows for the 3D and 2D growth regimes discussed above. To help interpretation of the growth mechanisms, the hydrogen desorption data in Fig. 2(b) are redrawn and overlapped with the growth rate characteristics in Fig. 4. Clearly, the 2D growth regime falls into the higher temperature part of the zone II region of Fig. 2(b), whereas the 3D growth regime falls into the zone III region. It should be mentioned that growth in the lower temperature part (550 to 710 °C) of zone II of Fig. 2(b) yields 3D columnar growth and inferior quality, and thus rarely applied in practical growth.[13] Such observation may give insight into the corre-

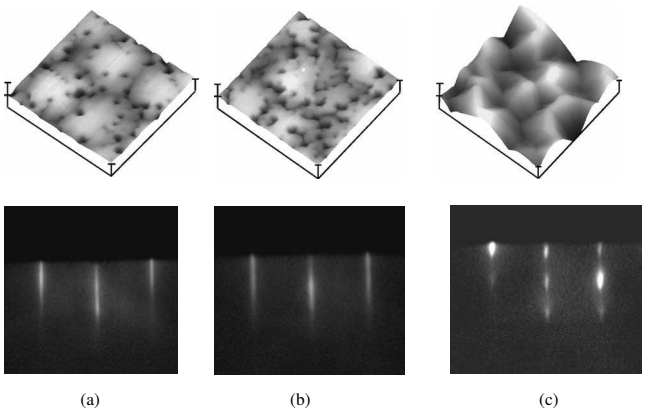

FIG. 5. *In situ* RHEED patterns and AFM surface images (1×1 μm^2 scan and 90 nm/div in vertical direction) for (a) sample A: semi-insulating UID GaN/SiC, (b) sample B: high-resistivity UID GaN/sapphire, and (c) sample C: conducting UID GaN/sapphire.

lation between the different surface kinetics (adsorption, cracking, desorption, and incorporation) and the mechanisms behind the different growth modes and the resultant electrical properties.

IV. HIGH-RESISTIVITY GAN VERSUS CONDUCTING GAN

In this section, we present a detailed comparison of the typical growth and material characterization results for semi-insulating (or high-resistivity) and conducting UID GaN by ammonia MBE. A carbon-doped semi-insulating GaN sample was also included in the study for comparison and interpretation purposes.

Semi-insulating (or high-resistivity) UID GaN layers have been successfully obtained on SiC (Cree semi-insulating 2″ wafer) and sapphire (2″ wafer) substrates using the 2D growth regimes described in Fig. 4. The growth parameters for the GaN growth are: 760 °C for growth temperature, 200 SCCM (BEP=1×10^{-4} Torr) for ammonia flux, 0.8 μm/hr for growth rate, and 1.3 μm for growth thickness. The conditions for the AlN buffer layer were given in the previous section about the experimental methods. One semi-insulating UID GaN sample grown on SiC is denoted as sample A. Another high-resistivity UID GaN sample grown on sapphire is denoted as sample B. For comparison, one n-type, conducting UID GaN sample, denoted as sample C, has been grown on a sapphire substrate using the 3D growth regime described in Fig. 4, with growth parameters being: 870 °C for growth temperature, 100 SCCM (BEP $=5\times10^{-5}$ Torr) for ammonia flux, 1 μm/hr for growth rate, and 1.3 μm for thickness. A carbon-doped semi-insulating GaN sample, denoted hereafter as sample D, was also grown in the 3D regime on a SiC substrate, using similar growth parameters as sample C. Details about carbon doping were published previously.[18]

Figure 5 shows *in situ* RHEED patterns and AFM surface images for samples A, B, and C. The RHEED patterns clearly show that the growth was 2D growth for the two highly resistive UID GaN samples A and B, and was 3D for the conducting sample C. From the AFM micrographs, the surfaces of samples A and B, with root-mean-square (rms) roughness of about 4 nm, are considerably smoother than that of sample C with rms roughness of 19 nm. Samples A and B basically show relatively flat (0001) surface with a quite high density of small pits which may be associated with the terminations of threading dislocations. In contrast, the surface of sample C shows dominant (10–1 m) pyramidal microfacets and vanishing (0001) top facet.

The surface kinetics discussed in the previous section may be part of the underlying reasons for the very different surface morphologies revealed in Fig. 5. The growth conditions for samples A and B falls into the zone II in Fig. 2(b), which is characterized by a nitrogen rich surface coverage. The high surface coverage of nitrogen species was further ensured by employing the maximum ammonia flow rate of 200 SCCM (BEP=1×10^{-4} Torr) designed for the MBE system. According to the kinetic model of Karpov *et al.*,[22] under such conditions, the adsorption sites are saturated and blocked by a layer of adsorbed NH_x radicals, preventing nitrogen atoms from evaporating (dissociation) from the step edges of the crystal. The adsorbed nitrogen species desorb slowly in the temperature range of zone II (550–800 °C) of Fig. 2(b), as can be seen by the low ammonia cracking rate on stationary GaN surface in Fig. 2(a). However, upon capturing Ga adatoms migrating to step edges, GaN incorporation via the $Ga+NH_x \Rightarrow GaN+H_2$ reaction occurs at a faster rate, which speeds up the nitrogen cracking processes and the refreshing rate of the adsorption sites following the GaN incorporation, making them available for adsorption of new ammonia molecules. That is why in the entire zone II, after the gallium flux is supplied to the GaN surface, the ammonia cracking rate is increased by an almost flat amount corresponding to the fixed Ga flux used. The growth temperature used (760 °C) is at the higher end of zone II, in order to provide sufficient surface mobility for Ga adatoms to diffuse to step edges, island edges where they can be attached to the lattice, and thus enabling 2D growth of the film. On the other hand, the growth temperature is still low enough, so that the step or nucleation island edges are still stable and saturated by adsorbed nitrogen species. Therefore, the kinetics in this regime is favorable for 2D nucleation and growth, resulting in smooth surface morphology. We find that UID GaN layers grown under such conditions on SiC or sapphire are electrically highly resistive, as will be characterized in detail in the next section.

On the other hand, the growth conditions with growth temperature at 870 °C for the conducting GaN sample C fall into the zone III of Fig. 2(b), where ammonia cracking rate on stationary GaN surface is significantly enhanced. The much enhanced cracking and desorption rate of the adsorbed nitrogen radicals indicates reduced blocking of adsorption and incorporation sites on the surface, and reduced blocking of nitrogen atoms escaping from crystal from step edges. This increases the likelihood of 3D nucleation and growth. At this high temperature range, the step edges are no longer thermally stable, and nitrogen atoms can easily decompose and dissociate from the edges. A consequence of the unstable step edge is that the Ga atoms can move up the edge, and react with nitrogen radicals to form a new layer on top. As a result, multilayers with closely bunched multiple steps are

TABLE I. SIMS measurement data for samples A: semi-insulating UID GaN/SiC, B: high-resistivity UID GaN/sapphire, C: conducting UID GaN/sapphire, and D: semi-insulating, carbon-doped GaN/SiC.

Sample	A	B	C	D
Oxygen (cm^{-3})	3×10^{17}	4×10^{17}	9×10^{17}	3×10^{18}
Carbon (cm^{-3})	8×10^{16}	6×10^{16}	8×10^{16}	3×10^{19}
Hydrogen (cm^{-3})	2×10^{18}	3×10^{18}	3×10^{18}	2×10^{19}

formed. In other words, the (0001) surface is no longer a stable facet under such conditions. The 3D growth involving creation of densely bunched steps eventually leads to dominating microfacets of the {10–1 m} pyramidal nature. As the AFM image for sample C shows, the (0001) top facet completely vanished on the surface. The pyramidal facets of course lead to significantly rougher surface than samples A and B grown under the 2D conditions. The UID GaN layers grown under the 3D growth conditions are found to be always conducting with electron concentrations usually in the range of 10^{16}–10^{17} cm^{-3} range.

In order to know impurity incorporation levels in UID GaN layers grown under the 2D and 3D conditions, we performed SIMS measurements for samples A, B, and C. Another carbon-doped GaN sample D was also included for comparison purpose. The results are presented in Table I. First, we notice that the oxygen levels in the 2D samples A and B are significantly lower than that in the 3D sample C. The carbon concentrations, on the other hand, are similar in all three samples. This trend is similar to what we reported in a previous study about growth regimes on SiC substrates.[24] This phenomenon suggests that oxygen incorporation is inhibited by the 2D surface kinetics, whereas carbon incorporation is insensitive to the surface kinetics. Under the 2D growth regime, the saturated coverage of adsorbed NH_x radicals in the adsorption layer likely blocks the adsorption and incorporation of oxygen atoms but cannot block the carbon species. Compared with the carbon doped GaN sample D, the oxygen and carbon concentrations in the UID GaN samples (A, B, and C) are lower by one order and more than two orders of magnitude, respectively. This confirms that the highly resistive property of the UID samples A and B is not simply due to impurities but rather caused by intrinsic defects as will be discussed in the next section. Of course, the reduced oxygen levels in samples A and B may have contributed to better carrier compensation in them.

We performed low temperature photoluminescence PL measurements on the four samples (A, B, C, and D) as described above. The low resolution and wide wavelength range PL spectra are shown in Fig. 6(a), and the high resolution PL spectra for the band-edge region in Fig. 6(b). The conducting GaN sample C shows the highest exciton emission intensity, whereas the highly resistive GaN samples A and B show reduced exciton peak intensity. The carbon-doped GaN sample (D), on the other hand, show nearly disappeared emission in the exciton region. The spectrum for the carbon-doped GaN sample is dominated by a broad yellow luminescence band. All the UID GaN samples, on the other hand, show much weaker yellow luminescence.

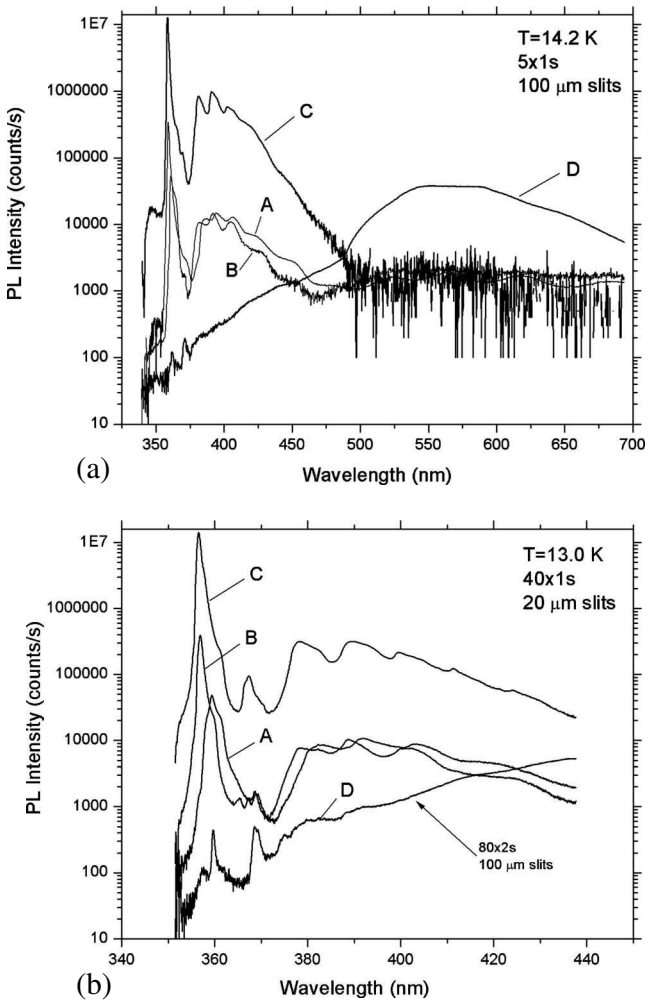

FIG. 6. Low temperature PL spectra: (a) low resolution and wide wavelength range, (b) high resolution in the band-edge region, for the four samples A: semi-insulating UID GaN/SiC, B: high-resistivity UID GaN/sapphire, C: conducting UID GaN/sapphire, and D: semi-insulating, carbon-doped GaN/SiC.

Several features can be observed by comparing the spectra. First, the PL properties of the highly resistive UID GaN samples are similar to those of the conducting UID GaN sample. Note that the slight shift of the exciton peak to higher wavelength for sample A is due to the tensile strain cause by the thermal mismatch with the SiC substrate used for this sample. All the UID samples show prominent exciton emissions and the well recognized shallow D-A pair emissions starting at about 3.28 eV. The yellow luminescence band is very weak in all the UID GaN samples. Common residual donors in ammonia MBE grown GaN include oxygen, silicon, and nitrogen vacancies.[30] Acceptors may result from carbon (C_N), nitrogen interstitial (N_I), and Ga vacancies etc.[31] The intensity of the exciton emission seems to relate inversely with the resistivity of the UID GaN. The most insulating sample A shows the lowest intensity. This suggests there are more abundant nonradiative recombination centers in the highly resistive materials, which may correlate with the deep centers that are also responsible for pinning the Fermi level in the semi-insulating materials. The PL intensity and resistivity do not seem to correlate in any obvious manner with the line defects in these samples. The

x-ray rocking curve full-width-at-half-maximum of the (0002) reflection are 633, 666, 446, and 360 arcsec for sample A, B, C, and D, respectively.

Second, we notice that the PL of the high-resistivity UID GaN is very different from that of the carbon-doped, high-resistivity GaN material. The carbon-doped material shows near complete quenching of the exciton emissions and the D-A pair emissions. Only the yellow luminescence band is observable even at such low temperature (10 K). The luminescence properties of the carbon-doped GaN have been reported and discussed in a previous paper.[9] Because of the high carbon (in the order of 10^{19} cm^{-3}) and associated oxygen (in the order of 10^{18} cm^{-3}) concentrations, radiative recombination of excitons is suppressed by prevailing nonradiative recombination centers that were introduced by the carbon-doping process. The nonradiative centers may involve carbon and oxygen impurities and their complexes formed with native defects. The yellow luminescence is the only remaining radiative recombination channel in the carbon-doped GaN material. There have been extensive research and debate on the origin of the notorious yellow luminescence (YL) in GaN. General consensus points to two possible transition mechanisms for the YL. The first ascribes the YL to a transition between shallow donors and a deep acceptor level about 0.9 eV above the valence band. The deep acceptors are formed by Ga vacancies (V_{Ga}), or more likely V_{Ga}–O_N complexes.[9,31–33] The second model ascribes the YL to a transition from the split deep levels (1.6 and 2.3 eV above valence band) formed by carbon interstitials (C_I) in carbon-doped GaN materials to shallow acceptors or the valence band.[34–36] Substitutional C_N atoms form shallow acceptor states at about 0.2 eV above the valence band.[37,38] Gallium vacancies/complexes are likely the dominant origin of YL in n-type GaN because the formation energy of V_{Ga} is lower when the Fermi level is near the conduction band.[31] Carbon impurities may be the dominant contributors to the YL in semi-insulating GaN where the Fermi level is lowered to midgap. Given the high carbon concentration of 10^{19} cm^{-3} in our sample D, it is very possible that most carbon atoms incorporated as interstitials, creating a large density of deep level defects, some of which contribute to the YL. The fact that the yellow luminescence is much stronger in the carbon-doped sample than in the UID samples may suggest much higher density of the carbon interstitials (C_I) in the former than the density of gallium vacancies in the latter. This is understandable given the carbon doping in the level of 10^{19} cm^{-3}. Native defects like gallium vacancies are unlikely to reach that level. Also the shallow donor to gallium vacancy (deep acceptor) transition depends on spatial overlap of the two centers. Relatively low densities of such centers, and thus large spatial separation between them, and competition from other recombination channels, may explain the weak yellow luminescence in the UID GaN samples here.

The carbon-related deep states can act both as radiative recombination centers and nonradiative recombination centers.[39] It has been observed that the impurities/defects responsible for the YL also shorten the lifetime of nonequilibrium carriers.[39] Such an interpretation is consistent with the PL spectrum of the carbon-doped GaN sample D. We see that the band-edge exciton emission as well as the shallow D-A pair emission is completely quenched, presumably by the carbon impurity nonradiative centers introduced at large densities, given the high carbon doping concentration in this sample.

The highly resistive and semi-insulating UID GaN, on the other hand, still shows dominant exciton emissions and D-A pair emissions. The shallow acceptor involved in the D-A pair emission is most likely C_N, since Mg doping had not been performed in our system for several years prior to this work. Because of significantly lower carbon concentrations in the order of 10^{16} cm^{-3}, C_N may account for a large portion of all the carbon atoms incorporated in the UID materials. This indicates that there are significantly fewer nonradiative centers in the high-resistivity UID material than in the carbon-doped material. The yellow luminescence in the UID material is also much weaker, consistent with the lower carbon incorporation level. In conclusion, compared with carbon-doped GaN, the high-resistivity UID GaN material is markedly cleaner in terms of impurities and defect centers, and is superior in optical properties and carrier lifetimes, and thus more suitable for use in active regions of certain device applications.

V. HIGH RESISTIVITY MEASUREMENT RESULTS

The layer grown on the SiC substrate, i.e., sample A, shows very good uniformity in electrical properties across the wafer. Figure 7(a) shows the dc dark current versus 1000/T characteristics measured with 100 V bias for two pieces (7×7 mm^2 in size), cut from the sample A. One piece used In contacts, while the other used annealed Ti/Al/Au metal contacts. The temperature dependent dc characteristics show well-defined activation energy of 1.02 eV. The room temperature resistivity is about 10^{11} Ω cm. Therefore, the UID GaN material grown on SiC is truly semi-insulating, with electrical conductivity governed by a deep level at 1.0 eV. On the other hand, the resistive UID GaN samples grown on sapphire substrates, i.e., the sample B and other similar samples, show quite significant nonuniformity, i.e., variation in resistivity across the wafer, and from wafer to wafer. This could be related to insufficient surface quality of the sapphire substrates, in spite of the substrate repolishing performed by Novasic Inc. Figure 7(b) shows several dc dark current versus 1000/T curves measured with 1 V bias on several pieces cut from sample B (piece B100608e) and other similarly grown samples (pieces B100408d and B140408). The room temperature resistivity varies from 10^6 to 10^9 Ω cm. And the measured resistivity activation energy in the high temperature range varied from 0.25, 0.52, to 0.90 eV. Therefore, such UID GaN layers grown on sapphire substrates are highly resistive but do not attain "semi-insulating" status. The resistivity is governed by gap states of varying depth (<0.9 eV) depending on incomplete compensation of electrically active impurities and dominant point-defect related deep centers, as observed by TSC characterization (see below).

Figures 8(a) and 8(b) show the photoconductivity response at 82 K for two pieces from the sample A, and several

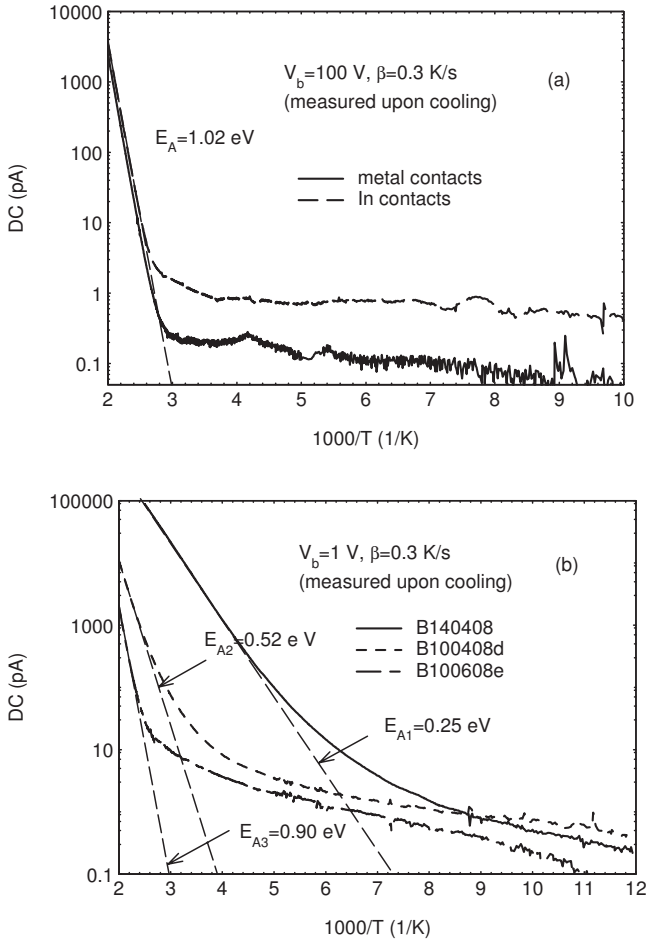

FIG. 7. (a) TDDC vs 1000/T characteristics measured with 100 V bias for two pieces from sample A (semi-insulating UID GaN/SiC), (b) TDDC vs 1000/T characteristics measured with 1 V bias for pieces from sample B (high-resistivity UID GaN/sapphire) and other similar UID GaN/sapphire sample.

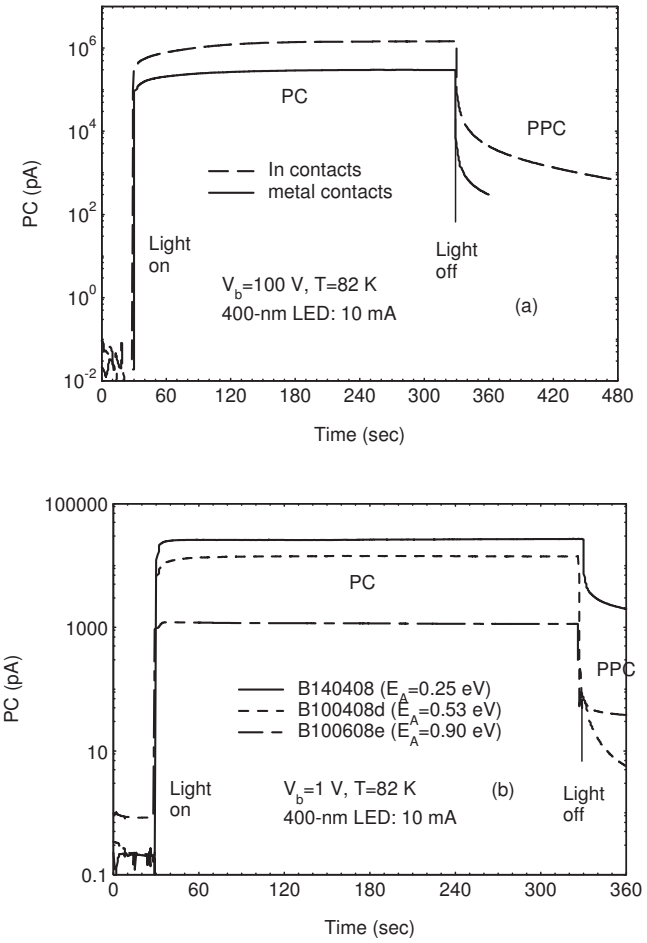

FIG. 8. The photoconductivity response at 82 K measured with 400 nm light for (a) two pieces from sample A (semi-insulating UID GaN/SiC), and (b) pieces from sample B (high-resistivity UID GaN/sapphire) and similar UID GaN/sapphire samples.

pieces from the sample B (piece B100608e) and wafers similar to sample B (pieces B100408d and B140408), respectively. The semi-insulating UID GaN pieces on SiC (sample A) show saturated photocurrent of 0.3–1.4 μA under 100 V bias and 400 nm light excitation. The high-resistivity UID GaN pieces, grown on sapphire (sample B and similar wafers) show saturated photocurrent of 1.1–20 nA under 1 V bias and 400 nm light excitation. It is important to note that the photo response (or photocurrent per 1 V) in both types of samples is many orders of magnitude higher than that in carbon-doped semi-insulating GaN materials. In a previous study,[9] the carbon-doped GaN layers showed saturated photocurrent of less than 0.2 pA under 100 V bias and 360 nm light excitation. This indicates that the UID semi-insulating/resistive GaN materials have significantly longer effective carrier lifetime than the carbon-doped GaN materials. This is consistent with the photoluminescence results in the previous section, which revealed the near complete quenching of excitonic emissions in the carbon-doped GaN. The density of deep traps and recombination centers must be significantly increased due to the heavy carbon doping to levels of 10^{19} cm^{-3}. Such deep centers could include carbon interstitials (C_I), $C_{Ga}-C_I$ complexes, or carbon-oxygen-point defects complexes.[34–36] In the UID semi-insulating/resistive GaN materials, the carbon concentrations are much lower, in the order of 10^{16} cm^{-3}. In this case, the carrier lifetime is much longer, and is limited mainly by intrinsic defects such as point defects. Long carrier lifetime is important for the efficiency of PIN diodes, Schottky diodes, and the base region of transistors, for example. Short carrier lifetime, on the other hand, is required for high speed operation of the devices. Therefore, in theory, it is possible to tune the carrier lifetime value in a wide range between the values for the resistive UID GaN and the heavily carbon-doped GaN. This offers an advantage from device design point of view.

Typical net TSC spectra for pieces from the sample A (with $E_A=1.0$ eV) and sample B (from piece B140408 with $E_A=0.25$ eV) are presented in Fig. 9, with TSC and dc shown together for comparison (note that net TSC=TSC-dc). The broad E-trap peak at ~100 K, is very prominent in the sample A, and exists also in the sample B. From the TSC peak temperature T_m for a given trap, an approximate activation energy can be determined from an equation $E_T = kT_m \ln(T_m^4/\beta)$, where k is Boltzmann's constant and β the heating rate (i.e., 0.3 K/s).[40] Trap E has activation energy of about 0.17 eV and has been identified with nitrogen vacancy in n-GaN layers by electron-irradiation study.[41] However, de-

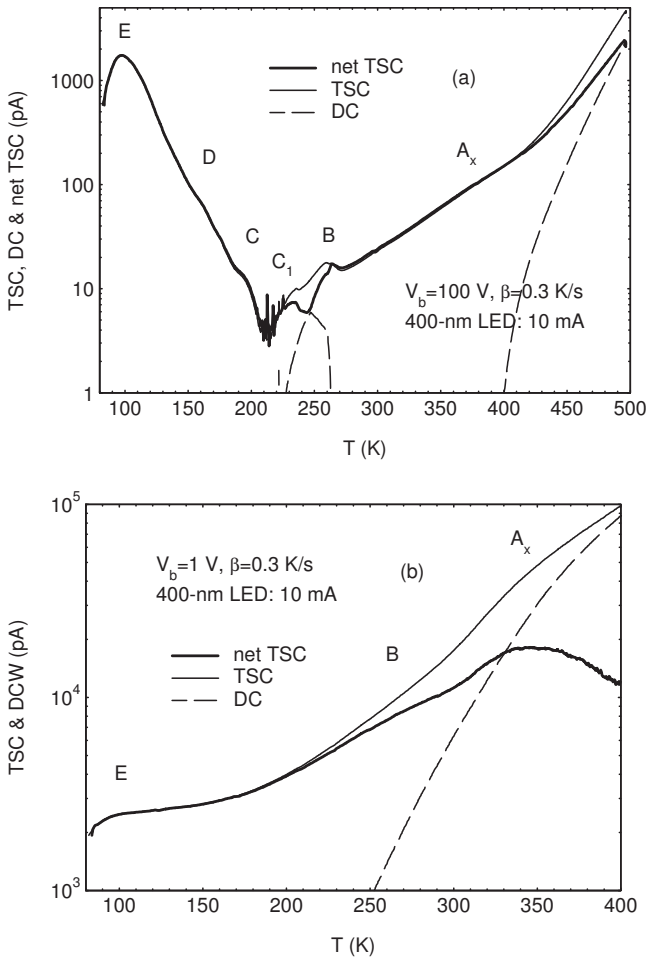

FIG. 9. Typical net TSC spectra measured at β=0.3 K/s for (a) sample A (semi-insulating GaN/SiC) with 100 V bias and 400 nm light, and (b) sample B (high-resistivity UID GaN/sapphire) with 1 V bias and 400 nm light. TSC and dc are also presented in the figures for comparison.

tailed data fittings have revealed that the broad E-band actually is the convolution of several traps E1 (0.07 eV), E2 (0.12 eV), E3 (0.21 eV), E4 (0.22 eV), and E5 (0.26 eV), among which E1 and E2 are electron traps, and E3–E5 are hole traps.[42] The hole traps E3–E5 might been attributed to C_N (Ref. 43) or V_{Ga}.[44] The TSC spectra also revealed traps B (0.52 eV) and A_x (0.74 eV) in both samples. The trap B, which is very weak in the samples A and B but is often the strongest trap in GaN grown by any method and not affected by electron-irradiation, could be due to C_{Ga} (Ref. 44) or Fe_{Ga}.[45] The trap A_x is close to the trap A (0.67 eV), which was observed in carbon doped GaN and has been associated with Ga vacancies in previous studies.[9] Other traps D (0.24 eV), C (0.30 eV), and C_1 (0.41 eV), which have been found in Fe-doped semi-insulating HVPE-grown GaN,[45] can be observed in the sample A, as shoulder features of the trap E.

In the following section, we attempt to interpret the nature of these dominant trap states, the correlation with the growth kinetics, and the effect on carrier compensation, transport, and recombination properties.

VI. INTERPRETATION OF COMPENSATION MECHANISMS

Attainment of semi-insulating status of "unintentionally doped" GaN requires a delicate balance among concentrations of "unintentional" donor and acceptor impurities, defects, and defect-related deep level (midgap). Unintentional donors may include oxygen (O_N), silicon (Si_{Ga}), nitrogen vacancies (V_N), carbon (C_{Ga}), etc. Unintentional acceptors may include carbon (C_N), Ga vacancies (V_{Ga}), other point defect-impurity complexes etc. Based on what has been observed in the present study, we propose that there is a 1.0 eV deep donor level ($E_C-1.0$ eV, denoted as "AY1" hereafter), and we tentatively attribute it to nitrogen antisite N_{Ga}. This deep level in GaN is assimilated to the well known "EL2" center (at $E_C-0.75$ eV) in unintentionally doped semi-insulating GaAs, where unintentional shallow acceptor is carbon and its concentration is higher than that of unintentional shallow donors. In fact, the 1.0 eV deep level has been observed in TDDC measurements of carbon-doped or Fe-doped semi-insulating GaN grown by MBE and HVPE.[9,45] The deep level, as an extended-defect related electron trap A_1, has been also widely observed by DLTS in n-type GaN and AlGaN/GaN heterostructures (for example, see Ref. 46). The results of the present work allude that this omnipresent native defect is very likely the nitrogen-antisite related defect, and it is the prominent native defect that controls the resistivity of unintentionally doped semi-insulating GaN, just like the EL2 defect (related to arsenic antisite) in unintentionally doped semi-insulating GaAs. Previous studies have also associated the nitrogen antisite defect (N_{Ga}) with deep states at 0.8–1.1 eV below the bottom of the conduction band,[47,48] which agrees well with the 1.0 eV activation energy found in our TDDC measurements of the semi-insulating materials.

If the concentration of the unintentional shallow donors is N_D, and the acceptors N_A, then the hope is that $N_A > N_D$ and existence of sufficient amount of the deep-donor levels, due to most prominently AY1 centers in the "unintentionally doped" GaN. Otherwise, the GaN would be p-type. When $N_{AY1} > N_A - N_D > 0$ is satisfied, the Fermi energy is controlled by the partially occupied AY1 states, and semi-insulating behavior results. We believe this scenario applies for the semi-insulating UID GaN grown on SiC, i.e., sample A. On the other hand, if the balance of compensation is such that $N_A - N_D < 0$, the Fermi energy will be controlled by shallower defect species rather than AY1, and the material will attain highly resistive status rather than semi-insulating. We believe this is the case for the high-resistivity UID GaN grown on sapphire substrates, i.e., sample B and similarly grown samples.

Experimentally we find there is a prominent trap E band in the TSC spectrum for sample A. The E band consists of electron and hole traps, resulting from shallow donors, such as V_N, and shallow acceptors, such as C_N and V_{Ga}. On the other hand, Ga vacancies or $V_{Ga}-O_N$ complexes can form deep acceptors at about 0.8–1.0 eV above the valence. The total of the shallow and deep acceptors seems to be sufficient to compensate all the unintentional shallow donors such as oxygen and nitrogen vacancies. As a result, the Fermi level is lowered to the 1 eV deep level AY1, the partial occupancy of which dictates the activation energy of the resistivity. From the SIMS data, we do observe the lowest oxygen concentration in the sample A. Although the measured oxygen concen-

tration is still higher than the carbon concentration, not all oxygen atoms incorporate as simple O_N donors. Some of them might contribute to $V_{Ga}-O_N$ acceptors, or incorporate in electrically inactive sites.

The TSC spectrum of sample B, on the other hand show only weak E band, which may indicate lower density of shallow acceptor-type defects. The carbon impurities may have incorporated as interstitials or other complexes rather than the C_N shallow acceptor. The oxygen concentration is higher and carbon concentration is lower in sample B. As a result, the compensation of shallow donors is incomplete. The PL results in Fig. 6 also show higher donor-bound exciton intensity for sample B than for sample A.

Finally, the growth kinetics can shed some light on why formation of acceptor-type defects and nitrogen antisites is favored in the specific growth regime applied, while donor impurities and defects are suppressed. The 2D growth regime used for the semi-insulating (or resistive) UID GaN materials is located in a particular temperature window, as marked in the growth characteristics graph in Fig. 4. The temperature window (740–780 °C) is located in the higher end of the growth kinetics zone II. A key feature for zone II is that the GaN surface is saturated with adsorbed ammonia molecules. The preferred adsorption sites are step edges, defects etc. In this temperature zone, adsorbed ammonia molecules, mostly in the form of NH_x radicals, crack thermally at a negligibly slow rate, if no incident gallium flux is applied to the surface. However, when an incident gallium flux is supplied to the surface, the ammonia cracking rate is increased by a significant amount that is proportional to the gallium flux. Obviously, the added ammonia cracking rate is due to the reaction between gallium and adsorbed ammonia species resulting in GaN lattice incorporation. It is anticipated such incorporation of gallium and nitrogen atoms occurs preferentially at step edges following diffusion of gallium adatoms. As a result, formation of GaN 2D nuclei and 2D growth/or step-flow growth can be maintained under such growth conditions. Another key factor is the high ammonia flux used. The V/III ratio, in terms of ammonia BEP (1×10^{-4} Torr) to gallium BEP (1×10^{-6} Torr) ratio, reaches 100:1. The high ammonia flux ensures saturated surface coverage of all available adsorption sites (e.g., step edges). With such a moderate growth temperature and saturated ammonia surface coverage, the key growth sites, namely the step edges, are thermally stable and blocked by adsorbed NH_x radicals. The blocking effect prevents nitrogen atoms from escaping the lattice from step edges,[22] thus reducing the chance of forming nitrogen vacancies, a donor type defect. From SIMS analysis, the blocking effect also reduces incorporation at step edges of oxygen, another donor impurity. On the contrary, the excess supply of nitrogen species at step edges encourages formation of Ga vacancies (an acceptor type defect), and nitrogen antisites (the 1.0 eV deep level defect). Therefore, we think the specific growth kinetics and conditions are responsible for the semi-insulating or highly resistive property of the UID GaN materials grown.

To explain why semi-insulating UID GaN is achieved only on SiC and the UID GaN layers grown on sapphire only achieved highly resistive status, we probably have to invoke the different lattice mismatch with the two substrates and the interplay with line defects. The larger lattice mismatch between GaN (AlN) and sapphire than with SiC can result in higher density of threading dislocations and difference in the nature of such line defects, i.e., screw type, edge type, or mixed type. Interplay of the line defects with point defects and impurities could have prevented formation of sufficient unintentional shallow C_N acceptors and deep gallium vacancy related "acceptors," or have produced excessive unintentional "donors," leading to not fully balanced compensation. Depending on the types and density of the dislocations, the unintentional carbon and oxygen atoms may preferentially decorate the core region of dislocations, forming complexes rather than substitutional shallow levels. Nevertheless, UID GaN with resistivity up to 10^9 Ω cm has been demonstrated on sapphire substrates as well.

In the end, we would like to comment on the conditions for growth of n-type conducting UID GaN. In Fig. 4, if we venture into the high temperature zone III, i.e., $T>820$ °C, the growth kinetics is markedly changed. At such high temperatures, the ammonia self cracking rate on the GaN surface is markedly enhanced [see Fig. 2(a)], and is no longer dependent on the supply of the Ga flux [see Fig. 2(b)]. This indicates that key surface features such as step edges are no longer thermally stable, and no longer effectively blocked by adsorbed ammonia species. In fact, kinetic roughening of an originally smooth GaN surface at such high temperature under an incident ammonia flux can be observed by *in situ* RHEED measurement. The surface roughening involves multiplication and bunching of steps, and eventually leads to facetted surface morphology as in Fig. 5(c). The kinetics is such that the growth mode is predominantly 3D facetted growth. The dense step edges on a facetted surface are favorable for nitrogen atoms to escape from the crystal, creating nitrogen vacancies. Such growth mode also promotes oxygen incorporation as confirmed by the SIMS data in Table I. Therefore the 3D growth regime in the zone III of the kinetics chart in Fig. 4 produces n-type GaN conducting materials with prevailing amount of donor-type defects and impurities, as opposed to smaller amount of unintentional acceptors and deep level defects. Because of the high growth temperature, the n-type conducting UID GaN, with electron density typically in the range of $10^{16}-10^{17}$ cm^{-3}, exhibits excellent crystal quality as well as optical and electrical properties, despite of a relatively rough surface morphology. Bulk mobilities as high as 560 $cm^2/V\,s$ have been reported for conducting GaN grown on sapphire substrates by ammonia MBE.[49] It is impossible to obtain high-resistivity UID GaN using the 3D regime in Fig. 4. However, it is possible to grow semi-insulating carbon-doped GaN in the 3D regime. In fact, excellent GaN/AlGaN HEMTs have been routinely grown in our laboratory using the 3D growth regime combined with a carbon-doped semi-insulating GaN buffer.[50,51] As discussed in the previous section, semi-insulating UID GaN or carbon-doped GaN each offers different advantages depending on specific device design for carrier lifetime, efficiency, speed, and interface quality etc.

VII. CONCLUSIONS

Growth of semi-insulating UID GaN on SiC and highly resistive UID GaN on sapphire by ammonia MBE has been demonstrated. The growth regime and mechanisms have been investigated and elucidated with experimental studies of the surface kinetics during growth. The growth regime requires a moderate temperature range (740–780 °C) and a high ammonia flux that ensures supersaturated adsorption coverage of the GaN surface. The key feature of the surface kinetics in this growth regime is that surface step edges are stable in this temperature range and that the step edges are blocked by adsorbed ammonia species which prevent nitrogen atoms from escaping the lattice. Ga adatoms diffuse and incorporate at step edges, leading to 2D layer by layer growth mode. Such nitrogen rich growth kinetics was found to reduce donor type oxygen impurity incorporation, and is expected to discourage donor type nitrogen vacancies while encourage acceptor type Ga vacancies and a deep center: nitrogen antisite N_{Ga}. The semi-insulating UID GaN on SiC exhibited a RT resistivity of 10^{11} Ω cm, and well defined activation energy of 1.0 eV. The 1.0 eV deep center is thought to be related to an intrinsic defect: the nitrogen antisite N_{Ga}, similar to the "EL2" center (related to As_{Ga}) in semi-insulating unintentionally doped GaAs. The semi-insulating behavior results from complete compensation of unintentional shallow donors by unintentional acceptors, and the Fermi level pinned to the partially occupied nitrogen antisite deep centers. The highly resistive UID GaN on sapphire exhibited RT resistivity in a range from 10^6 to 10^9 Ω cm and activation energy varying from 0.25 to 0.9 eV. The high resistivity behavior results from incomplete compensation of shallow donors, and the Fermi level controlled by levels shallower than the 1.0 eV deep nitrogen antisite center. The semi-insulating or highly resistive UID GaN exhibits orders of magnitude longer effective carrier lifetime than the semi-insulating carbon-doped GaN. Therefore semi-insulating UID GaN can offer advantages in certain device applications such as PIN diodes, Schottky diodes, photoconductors, etc, when high efficiencies are required. On the other hand, as a lifetime shortening dopant, carbon-doping may be used to tune the carrier life time to desired values, when fast switching speed is required for certain applications.

ACKNOWLEDGMENTS

The authors are indebted to S. Moisa and I. Sproule for SIMS measurements, G. Parent for AFM measurements, and L. Polenta for fitting the TSC measurement data.

[1]R. P. Vaudo, X. Xu, A. Salant, J. Malcarne, and G. R. Brandes, Phys. Status Solidi A **200**, 18 (2003).
[2]J. A. Freitas, Jr., J. G. Tischlera, J.-H. Kimb, Y. Kumagaic, and A. Koukituc, J. Cryst. Growth **305**, 403 (2007).
[3]S. Heikman, S. Keller, S. P. DenBaars, and U. K. Mishra, Appl. Phys. Lett. **81**, 439 (2002).
[4]A. E. Wickenden, D. D. Koleske, R. L. Henry, M. E. Twigg, and M. Fatemi, J. Cryst. Growth **260**, 54 (2004).
[5]M. Azize, M. Leroux, M. Laugt, P. Gibart, and Z. Bougrioua, Phys. Status Solidi A **203**, 1744 (2006).
[6]A. Corrion, F. Wu, T. Mates, C. S. Gallinat, C. Poblenz, and J. S. Speck, J. Cryst. Growth **289**, 587 (2006).
[7]F. Mei, Q. M. Fu, T. Peng, C. Liu, M. Z. Peng, and J. M. Zhou, J. Appl. Phys. **103**, 094502 (2008).
[8]H. Tang, J. B. Webb, J. A. Bardwell, S. Raymond, J. Salzman, and C. Uzan-Saguy, Appl. Phys. Lett. **78**, 757 (2001).
[9]Z.-Q. Fang, D. C. Look, B. Claflin, S. Haffouz, H. Tang, and J. Webb, Phys. Status Solidi C **2**, 2757 (2005).
[10]M. J. Manfra, N. G. Weimann, J. W. P. Hsu, L. N. Pfeiffer, K. W. West, and S. N. G. Chu, Appl. Phys. Lett. **81**, 1456 (2002).
[11]P. Kordos, P. Javorka, M. Morvic, J. Betko, J. M. Van Hove, A. M. Wowchak, and P. P. Chow, Appl. Phys. Lett. **76**, 3762 (2000).
[12]M. Micovic, A. Kurdoghlian, P. Janke, P. Hashimoto, D. W. S. Wong, J. S. Moon, L. McCray, and C. Nguyen, IEEE Trans. Electron Devices **48**, 591 (2001).
[13]A. L. Corrion, C. Poblenz, F. Wu, and J. S. Speck, J. Appl. Phys. **103**, 093529 (2008).
[14]W. Kim, O. Aktas, A. Salvador, A. Botchkarev, B. Sverdlov, S. N. Mohammad, and H. Morkoc, Solid-State Electron. **41**, 169 (1997).
[15]F. Semond, P. Lorenzini, N. Grandjean, and J. Massies, Appl. Phys. Lett. **78**, 335 (2001).
[16]N. Baron, Y. Cordier, S. Chenot, P. Vennéguès, O. Tottereau, M. Leroux, F. Semond, and J. Massies, J. Appl. Phys. **105**, 033701 (2009).
[17]Y. Cordier, F. Semond, M. Hugues, F. Natalie, P. Lorenzini, H. Haas, S. Chenot, M. Laugt, O. Tottereau, P. Vennegues, and J. Massies, J. Cryst. Growth **278**, 393 (2005).
[18]J. B. Webb, H. Tang, S. Rolfe, and J. Bardwell, Appl. Phys. Lett. **75**, 953 (1999).
[19]V. K. Gupta, K. L. Averett, M. W. Koch, B. L. Mcintyre, and G. W. Wicks, J. Electron. Mater. **29**, 322 (2000).
[20]M. Mesrine, N. Grandjean, and J. Massies, Appl. Phys. Lett. **72**, 350 (1998).
[21]D. E. Crawford, R. Held, A. M. Johnston, A. M. Dabiran, and P. I. Cohen, MRS Internet J. Nitride Semicond. Res. **1**, 12 (1996).
[22]S. Y. Karpov, R. A. Talalaev, Y. N. Makarov, N. Grandjean, J. Massies, and B. Damilano, Surf. Sci. **450**, 191 (2000).
[23]R. Held, D. E. Crawford, A. M. Johnston, A. M. Dabiran, and P. I. Cohen, Surf. Rev. Lett. **5**, 913 (1998).
[24]H. Tang, S. Rolfe, F. Semond, J. A. Bardwell, and J. M. Baribeau, J. Cryst. Growth **311**, 2091 (2009).
[25]J. B. Webb, H. Tang, J. A. Bardwell, S. Moisa, C. Peters, and T. MacElwee, J. Cryst. Growth **230**, 584 (2001).
[26]H. Tang, J. B. Webb, J. A. Bardwell, S. Rolfe, and T. MacElwee, Solid-State Electron. **44**, 2177 (2000).
[27]N. Grandjean and J. Massies, Appl. Phys. Lett. **71**, 1816 (1997).
[28]N. Grandjean and J. Massies, Appl. Phys. Lett. **73**, 1260 (1998).
[29]N. Grandjean, J. Massies, I. Grzegory, and S. Porowski, Semicond. Sci. Technol. **16**, 358 (2001).
[30]D. C. Look, D. C. Reynolds, J. W. Hemsky, J. R. Sizelove, R. L. Jones, and R. J. Molnar, Phys. Rev. Lett. **79**, 2273 (1997).
[31]J. Neugebauer and C. G. Van de Walle, Appl. Phys. Lett. **69**, 503 (1996).
[32]T. Ogino and M. Aoki, Jpn. J. Appl. Phys., Part 1 **19**, 2395 (1980).
[33]D. M. Hofmann, D. Kovalev, G. Steude, B. K. Meyer, A. Hoffmann, L. Eckey, R. Heitz, T. Detchprom, H. Amano, and I. Akasaki, Phys. Rev. B **52**, 16702 (1995).
[34]R. Armitage, W. Hong, Q. Yang, H. Feick, J. Gebauer, E. R. Weber, S. Hautakangas, and K. Saarinen, Appl. Phys. Lett. **82**, 3457 (2003).
[35]W. You, X. D. Zhang, L. M. Zhang, Z. Yang, H. Bian, Q. Ge, W. X. Guo, W. X. Wang, and Z. M. Liu, Physica B **403**, 2666 (2008).
[36]A. F. Wright, J. Appl. Phys. **92**, 2575 (2002).
[37]H. Wang and A.-B. Chen, Phys. Rev. B **63**, 125212 (2001).
[38]A. Armstrong, A. R. Arehart, B. Moran, S. P. DenBaars, U. K. Mishra, J. S. Speck, and S. A. Ringel, Appl. Phys. Lett. **84**, 374 (2004).
[39]J. Mickevièius, R. Aleksiejunas, M. S. Shur, S. Sakalauskas, G. Tamulaitis, Q. Fareed, and R. Gaska, Appl. Phys. Lett. **86**, 041910 (2005).
[40]D. C. Look, Semicond. Semimetals **19**, 75 (1983).
[41]Z.-Q. Fang, J. W. Hemsky, D. C. Look, and M. P. Mack, Appl. Phys. Lett. **72**, 448 (1998).
[42]L. Polenta and Z.-Q. Fang (unpublished).
[43]S. Fischer, C. Wetzel, E. E. Haller, and B. K. Meyer, Appl. Phys. Lett. **67**, 1298 (1995).
[44]D. C. Look, Z.-Q. Fang, and B. Claflin, J. Cryst. Growth **281**, 143 (2005).
[45]Z. Q. Fang, B. Claflin, D. C. Look, S. Elhamri, H. E. Smith, W. C. Mitchel, D. Hanser, E. A. Preble, and K. R. Evans, Phys. Status Solidi C **5**, 1508 (2008).

[46]Z.-Q. Fang, D. C. Look, D. H. Kim, and I. Adesida, Appl. Phys. Lett. **87**, 182115 (2005).
[47]T. L. Tansley and R. J. Egan, Physica B **185**, 190 (1993).
[48]T. Suski, P. Perlin, H. Teisseyre, M. Leszczynski, I. Grzegory, J. Jun, and M. Bockowski, Appl. Phys. Lett. **67**, 2188 (1995).
[49]H. Tang and J. Webb, Appl. Phys. Lett. **74**, 2373 (1999).
[50]J. B. Webb, H. Tang, J. A. Bardwell, and P. Coleridge, Appl. Phys. Lett. **78**, 3845 (2001).
[51]J. A. Bardwell, Y. Liu, H. Tang, J. B. Webb, S. J. Rolfe, and J. Lapointe, Electron. Lett. **39**, 564 (2003).